Published in final edited form as:
Transl Neurosci. 2013 March 1; 4(1): 8–19. doi:10.2478/s13380-013-0111-8.

REGION-SPECIFIC NEURON AND SYNAPSE LOSS IN THE HIPPOCAMPUS OF APP^{SL}/PS1 KNOCK-IN MICE

Ivona Brasnjevic[1,2,#], **Roy Lardenoije**[1,#], **Christoph Schmitz**[3], **Nicolien Van Der Kolk**[1,2], **Dara L. Dickstein**[4], **Hisaaki Takahashi**[5], **Patrick R. Hof**[4], **Harry W.M. Steinbusch**[1,2], and **Bart P.F. Rutten**[1,2]

Bart P.F. Rutten: b.rutten@maastrichtuniversity.nl

[1]Department of Psychiatry and Neuropsychology, Maastricht University, 6200 MD Maastricht, The Netherlands [2]European Graduate School of Neuroscience (EURON), 6200 MD Maastricht, The Netherlands [3]Department of Anatomy II, Institute of Anatomy, Ludwig-Maximilians-University, 80336 Munich, Germany [4]Fishberg Department of Neuroscience and Friedman Brain Institute, Icahn School of Medicine at Mount Sinai, New York, NY 10029, USA [5]Department of Molecular and Cellular Physiology, Graduate School of Medicine, Ehime University, 791-0295 Ehime, Japan

Abstract

Transgenic mouse models with knock-in (KI) expression of human mutant amyloid precursor protein (APP) and/or human presenilin 1 (PS1) may be helpful to elucidate the cellular consequences of APP and PS1 misprocessing in the aging brain. Age-related alterations in total numbers of neurons and in numbers of synaptophysin-immunoreactive presynaptic boutons (SIPB), as well as the amyloid plaque load were analyzed in the hippocampal dentate gyrus (DG), CA3, and CA1–2 of 2- and 10-month-old APP^{SL}/PS1 homozygous KI, APP^{SL} (expressing human mutant APP751 carrying the Swedish [K670N/M671L] and London [V717I] mutations under Thy-1 promoter), and PS1 homozygous KI mice (expressing human PS1 mutations [M233T and L235P]). APP^{SL}/PS1 homozygous KI mice, but neither APP^{SL} mice nor PS1 homozygous KI mice, showed substantial age-related loss of neurons (−47.2%) and SIPB (−22.6%), specifically in CA1–2. PS1 homozygous KI mice showed an age-related increase in hippocampal granule cell numbers (+37.9%). Loss of neurons and SIPB greatly exceeded the amount of local extracellular Aβ aggregation and astrocytes, whereas region-specific accumulation of intraneuronal Aβ preceded neuron and synapse loss. An age-related increase in the ratio of SIPB to neuron numbers in CA1–2 of APP^{SL}/PS1 homozygous KI mice was suggestive of compensatory synaptic plasticity. These findings indicate a region-selectivity in intra- and extraneuronal Aβ accumulation in connection with neuron and synapse loss in the hippocampus of APP^{SL}/PS1 homozygous KI mice.

Correspondence to: Bart P.F. Rutten, b.rutten@maastrichtuniversity.nl.
[#]equal contributions

Keywords

Alzheimer's disease; Amyloid precursor protein; Neuron loss; Synapse loss; Hippocampus; Presenilin-1; Stereology; Image analysis

1. Introduction

The mechanistic relationships among the neuropathologic hallmarks of Alzheimer's disease (AD) remain incompletely understood. Early synaptic dysfunction and neuron loss in hippocampal and neocortical circuits are nowadays considered the strongest correlates of cognitive decline in AD [1–4]. Supported by compelling genetic data on early-onset familial AD, the amyloid beta-peptide (Aβ)-centric theory holds that Aβ is involved in the pathogenesis of sporadic AD [2,5], although in recent years this view has been challenged [6,7]. While different species and forms of Aβ aggregates exist, $A\beta_{42}$ has recently been suggested to be the most pathogenic [8]. In addition, differential toxicity may exist between extracellular aggregates of thioflavin S-positive plaques, soluble Aβ aggregations in the form of oligomers, and intracellular Aβ species [9–11].

The elucidation of the cascade of events and the contribution of human mutant amyloid precursor protein (APP), human presenilin 1 (PS1), and the various species and forms of Aβ to age-related neuron and synapse loss is far from conclusive [12–18]. Our initial study on 4.5- and 17-month-old double transgenic $APP751^{SL}/PS1^{M146L}$ mice revealed significant age-related loss of synaptophysin-immunoreactive presynaptic boutons (SIPB) extending beyond the regions of extracellular Aβ deposits but in association with intraneuronal Aβ [15]. Moreover, a 30% loss of hippocampal neurons in 17-month-old $APP751^{SL}/PS1^{M146L}$ mice ($APP751^{SL}$ mice that carry the Swedish and London mutations KM670/671NL and V717I under the control of the Thy-1 promoter together with human mutant PS1 M146L under the control of the HMG promoter) was shown to be largely plaque-independent [11], reinforcing the idea of complex interactions between neuron loss, Aβ deposits, intraneuronal Aβ, and PS1-mediated effects on hippocampal synaptic and neuronal integrity.

To gain further insight into the mechanistic relationship between neuron and synapse loss, as well as the impact of mutant PS1 on impairments of synaptic function apart from its contribution to altered APP processing and Aβ generation, we used in the present study the homozygous APP^{SL}/PS1ho KI mouse model, that express two mutations in the human APP gene as well as two human PS1 mutations knocked-in into the mouse PS1 gene in a homozygous (ho) manner. Coexpression of M233T/L235P mutations into the endogenous PS1 locus potentiates pathology to the extent that some lines begin to develop intraneuronal Aβ at about 2 months of age [19], followed by the development of neuritic plaques in neocortex and hippocampus and impairment of cognitive function at the age of 6 months, as revealed using the Y-maze and the T-maze continuous alteration task [20]. Major deficits in long-term potentiation (LTP) have also been reported in the APP^{SL}/PS1ho KI mice, as early as 6 months of age [19–21]. The APP^{SL}/PS1ho KI model is of particular interest as it exhibits substantial age-related neuron loss in the pyramidal layer of the hippocampus (up to 50%) [22], a finding supporting the notion that intraneuronal Aβ-species may posses toxic

properties. However, the regional and temporal pattern of neuron and synapse loss in this model has not been described in detail.

The present study was designed to test the hypothesis that coexpression of human APP^{SL} with PS1 under the endogenous mouse promoter results in age-related loss of neurons and synapses in a hippocampal region-specific manner. We investigated age-related changes in the total numbers of neurons, SIPB, as well as the accumulation of intraneuronal and extracellular Aβ in the hippocampus of various strains of the APP^{SL}/PS1 KI mouse model using design-based stereology and quantitative neuroanatomical techniques.

2. Experimental Procedures

2.1 Animals

The following groups of 2-month-old (M2) and 10-month-old (M10) mice were obtained from Sanofi-Aventis Centre de Recherche de Paris (Vitry sur Seine, France): APP mice (transgenic mice expressing human mutant APP751 carrying the Swedish [K670N/M671L] and London [V717I] mutations; mouse Thy-1 promoter) (n = 9; 6 males, 3 females), PS1ho mice (expressing human PS1 mutations [M233T and L235P] knocked-in into the mouse PS1 gene in a homozygous manner) (n = 9; 7 males, 2 females), and APP/PS1KI mice (expressing both the aforementioned APP and PS1ho mutations) (n = 8; 5 males, 3 females). In the case of APP^{SL}/PS1ho KI mice, an additional group of 6-month-old (M6) mice was included in the study (n = 5; 4 males, 1 female). A detailed description of these mice was reported earlier [19,22]. Due to the complicated genetic background of these mice, we could not include wild-type mice in the present study. All experiments were approved by the Aventis Animal Care and Use Committee, in accordance with standards for the care and use of laboratory animals formulated by the French and European Community (Centre National de la Recherche Scientifique - Institute of Laboratory Animal Resources).

2.2 Tissue Processing

Mice were anesthetized and perfused transcardially as previously described [11]. The brains were rapidly removed from the skulls and halved in the sagittal plane. The left hemispheres were cryoprotected by immersion in 30% sucrose, quickly frozen and cut into series of 30 μm-thick coronal sections. These series of sections were then divided into subseries of every 10th section, yielding 10 series of 5 to 8 sections containing the whole hippocampus in each animal. From these materials, three 1:10 series of sections from the left hemisphere of each animal were used for different experimental purposes.

One series was mounted on glass slides, dried, defatted with Triton X-100 (0.025%, 20 min; Merck, Darmstadt, Germany) and stained with cresyl violet (0.01%, 15 min). A second series was used for immunohistochemical detection of synaptophysin (mouse monoclonal anti-synaptophysin antibody; 1:2,000; Chemicon, Souffelweyersheim, France; avidin-biotin immunoperoxidase labeling) as previously described [15]. The Mouse-On-Mouse immunodetection kit (Vector Laboratories, Peterborough, UK) was used according to the manufacturer's protocol to minimize background labeling and labeling of intraparenchymal IgG molecules. Control experiments comprised incubations without primary antibody and

incubations without use of the Mouse-On-Mouse immunodetection kit (Vector Laboratories). All incubations were performed with free-floating sections under exactly identical conditions. After immunohistochemical procedures, sections were mounted on gelatinized glass slides, dehydrated, coverslipped, and coded. The code was not broken until all analyses were completed.

A third series was used for immunohistochemical detection and quantification of Aβ and glial fibrillary acidic protein (GFAP) as recently described [11]. Immunohistochemistry on free-floating sections was performed using standard immunofluorescence labeling procedures. Briefly, sections were washed 3×15 minutes in 0.1 M Tris-buffered saline (TBS, pH 7.6), with the addition of 0.3% Triton X-100 (TBS-T), preincubated at room temperature (20°C). Sections were then treated with 10% fetal calf serum and 4% non-fat-dry-milk in TBS, to block non-specific binding sites, and then incubated overnight at 4°C in the following primary antibodies: monoclonal mouse anti-GFAP IgG1 clone G-A-5 (Sigma, St. Louis, MO, USA, catalog #G3893, dilution 1:1,600) raised against purified GFAP from pig spinal cord and rabbit anti-mouse polyclonal antiserum 730 (against human Aβ and P3; generously provided by Dr. Gerd Multhaup; [21,23], dilution 1:1,500) raised against a synthetic peptide corresponding to human $A\beta_{-40}$. Following incubation in primary antibody, the sections were rinsed 3×15 minutes in TBS and incubated with secondary antibodies for 1.5 hours at room temperature. Donkey anti-mouse IgG Alexa Fluor 488 (1:100; Molecular Probes, Eugene, OR, USA) and donkey anti-rabbit IgG Alexa Fluor 594 (1:100; Molecular Probes) were used as secondary antibodies. Sections were washed, counterstained with Hoechst 33342 (1:500; Sigma), mounted on glass slides and coverslipped with 80% glycerol-TBS. The expected cellular morphology and distribution of staining for each primary antibody were consistent with earlier studies. All secondary antibody combinations were carefully examined to ensure that there was no crosstalk between fluorescent dyes or cross-reactivity between secondary antibodies.

2.3 Stereologic analyses

Stereologic analyses were carried out using a computer-based stereology workstation consisting of a modified light microscope (Olympus BX50 with UPlanApo objectives 10× [N.A. = 0.4], 20× [oil; N.A. = 0.7], 40× [oil; N.A. = 1.0], and 100× [oil; N.A = 1.35]; Olympus, Tokyo, Japan), a motorized specimen stage for automatic sampling (Ludl Electronics, Hawthorne, NY, USA), a focus drive linear encoder (Ludl Electronics), a CCD color video camera (HVC20AMP; Hitachi, Tokyo, Japan), and stereology software (StereoInvestigator v. 7.00.03; MBF Bioscience, Williston, VT, USA).

The sections stained with cresyl violet were used to estimate the volumes of the following regions in the hippocampus with the Cavalieri principle (as shown in Figure 2 in [24]: *stratum moleculare* of the DG (SM), *stratum lucidum* of CA3 (SL), and *stratum radiatum* of CA1–2 (SR). Estimates were obtained with a 10× objective by tracing the boundaries of these regions according to Franklin and Paxinos [25] on video images displayed on the computer screen.

The same sections were used to estimate total numbers of neurons in DG, CA3, and CA1–2 with the Optical Fractionator (see Figures 1 and 4 in [24]). All neurons whose nucleus top

came into focus within unbiased virtual counting spaces distributed in a systematic-random fashion throughout the regions of interest were counted. Estimated total neuron numbers were calculated from the number of counted neurons and the sampling probability (all details of the counting procedure are summarized in Table 1).

Finally, the sections processed for the detection of Aβ and GFAP were used to determine the amount of extracellular Aβ aggregates in the different regions of the hippocampus. Estimates were obtained with point counting and results from the sections immunoprocessed for the detection of Aβ and GFAP were used to calculate 'reconstructed' numbers of neurons as previously described [11], assuming that the space within a given region in the hippocampus occupied by extracellular Aβ aggregates and surrounding astrocytes would have contained neurons at the same mean neuronal density as the other parts of this region. The unreconstructed numbers of neurons that were used to determine the mean neuronal density of a region were estimated as described above. The reconstructed numbers of neurons were used throughout the study and referred to as the total number of neurons.

2.4 Image analysis

The sections immunohistochemically labeled for synaptophysin were used to determine the SIPB densities in regions of the hippocampus mentioned above as described in [15]. Briefly, five high-resolution photomicrographs were taken from each selected area at about 2 μm below the upper surface of the sections (*i.e.*, when the SIPB were clearly in focus) with a digital camera (F-view, Olympus) attached to an Olympus AX-70 microscope (UPlanApo objectives 100× [oil; N.A = 1.35]; Olympus). In the case of the APP^{SL} and the APP^{SL}/PS1ho KI mice, photomicrographs were taken exclusively from regions free of Aβ deposits and Aβ aggregation-related alterations of normal SIPB morphology. Aβ deposits were clearly recognizable as round or oval structures not immunoreactive for synaptophysin and surrounded by multiple enlarged SIPB and disturbed neuropil.

SIPB were detected by an image analysis system using AnalySIS-pro software (Soft Imaging System, Münster, Germany), slightly modified for detection of grayscale puncta as previously described [15,26]. All measurements were performed on a single focal plane. Shading error correction was performed before measurements to correct for irregularities in illumination of the microscopic field. Furthermore, background levels were equalized. The detection thresholds were tested in a pilot experiment; corresponding values were stored in the computer program and kept at the same levels for all samples. From these data, SIPB density per μm^2 was calculated in each area for each section. The procedure resulted in 75–120 photomicrographs for SM, SL, and SR per animal (5 photomicrographs × 3 areas × 5 to 8 sections). The mean SIPB density was calculated per region in each animal.

2.5 Calculation of SIPB numbers and SIPB-to-neuron ratio

Total uncorrected SIPB numbers were calculated by multiplying the SIPB densities with the corresponding volume data in each animal. To take the impact of Aβ deposits on SIPB numbers into account, the percent volume occupied by Aβ deposits and Aβ aggregation-related alterations in SIPB morphology in SM, SL, and SR was subtracted from the total volume of the investigated hippocampal subregions. Multiplying these values by the

corresponding SIPB densities resulted in corrected SIPB numbers, which were used throughout the study and referred to as total SIPB numbers.

Because SIPB densities were analyzed in one focal plane, it should be noted that the calculated SIPB numbers are not unbiased [24]. The calculations did not take the dimensions of the investigated parameter, *i.e.* $1/\mu m^2$ (SIPB density) and mm^3 (volume) into account. Distribution plots for SIPB size were obtained [15]. These plots were comparable among animals, and the average SIPB size was not dependent on the plane of section.

SIPB-to-neuron ratios were obtained for each animal by dividing the corrected total SIPB numbers with the reconstructed total number of neurons per hippocampal subregion. Note that this ratio is dimensionless as it is obtained from calculated SIPB numbers.

2.6 Statistical analysis

For all groups of mice, means and standard error of the mean were calculated for all measured variables. Generalized linear model univariate analysis of variance, with age and genotype as fixed factors, was performed to compare effects on volumes, total numbers of neurons, and total SIPB number. When statistically significant differences were found in the univariate analysis of variance calculations, data from the 2-month-old animals were compared with the corresponding data from the 10-month-old animals (and, in the case of APP^{SL}/PS1ho KI mice, to 6-month-old animals as well) of the same genotype with Bonferroni post-hoc tests. Statistical analyses for SIPB-to-neuron ratio were only carried out for animals with observed age-related changes in total neuron or SIPB numbers. Effects were considered statistically significant if their associated p value was smaller than 0.05. Calculations were performed using SPSS (v. 12.0.1 for Windows; SPSS, Chicago, IL, USA). Graphs were constructed using GraphPad Prism (v. 4.00 for Windows; GraphPad Software, San Diego, CA, USA).

2.7 Photography

Photomicrographs were produced by digital photography using an Olympus DP 70 digital camera attached to an Olympus AX 70 microscope and cellP software (v. 2.3; Soft Imaging System, Münster, Germany). The final figures were constructed using Adobe Photoshop CS5.1 (Adobe Systems, San Jose, CA, US). Only minor adjustments of contrast and brightness were made, without altering the appearance of the original materials.

3. Results

Table 2 summarizes the p values of the generalized linear model univariate analysis of variance for volumes, total numbers of neurons, and total SIPB numbers.

3.1 Age-related reductions in regional volumes in the hippocampus of APP^{SL}/PS1ho KI mice

Generalized linear model univariate analyses showed a significant effect of age, but no significant effects of genotype, or interactive effects of age and genotype, on the volume of SR of CA1–2. No significant effects were found for volumes of SM of the DG and SL of

CA3. Adding animal's sex as covariate did not change the results. Bonferroni post-hoc tests indicated age-related reductions in volumes of SM and SR between 2-month-old and 10-month-old APP^{SL}/PS1ho KI mice (SM: −23.7%, p = 0.049, and SR: −31.8%, p = 0.001; Figure 1).

3.2 Region-specific differences in immunohistochemical detection of Aβ aggregates

Quantifications showed a relative amount of extracellular Aβ aggregates and surrounding astrocytes in the cell layers of 0.7% in DG, 0.2% in CA3, and 0.2% in CA1–2 of 10-month-old APP^{SL} mice, and 6.4% in DG, 6.1% in CA3, 4.3% in CA1–2 in 10-month-old APP^{SL}/PS1ho KI mice (Figure 2; plaque load data for white matter regions are provided separately). PS1ho KI mice did not exhibit extracellular Aβ aggregates.

3.3 Age-related changes in total numbers of neurons

Generalized linear model univariate analyses showed significant effects of age on total number of neurons of neurons in CA1–2, of genotype on total number of neurons in DG and CA1–2, and the interaction between age and genotype on total number of neurons in CA1–2. Adding sex as covariate did not change the results. At the age of 2 months, the total number of neurons did not differ between APP^{SL}, PS1ho KI and APP^{SL}/PS1ho KI mice in any hippocampal region. Bonferroni post-hoc tests indicated an age-related increase in total number of neurons in DG of PS1ho KI mice (+37.9%, p = 0.006), while a decrease of 47.2% was found for the total neuron number in 10-month-old CA1–2 APP^{SL}/PS1ho KI mice compared to 2-month-old animals (p = 0.002, Figures 3D–F, 4, 5 and Table 2). The means of total number of neurons in CA1–2 in 6-month-old APP^{SL}/PS1ho KI mice were directionally lower (but not statistically significant) as compared to 2-month-old mice (−17.9%; p = 0.267, Figure 6B). Means and standard errors of uncorrected total neuron numbers are given in Figure 7.

3.4 Alterations in SIPB morphology due to Aβ deposits

Regions directly adjacent and surrounding the Aβ deposits showed overt morphological alterations in synaptophysin immunoreactivity, while no synaptophysin immunoreactivity was observed within the core of the Aβ deposits (Figure 8). As in our previous study [15], we observed considerably enlarged SIPBs close to the Aβ deposits in the brain of APP^{SL} mice and APP^{SL}/PS1ho KI mice (Figure 8).

3.5 Age-related reductions in SIPB numbers in CA1–2 of APP^{SL}/PS1ho KI mice

Generalized linear model univariate analyses showed significant effects of genotype on total SIPB number in SM and SR, and of the interaction between age and genotype on total SIPB number in SM. Adding sex as covariate did not change the results. Bonferroni post-hoc tests on total SIPB numbers in SM and SL did not show significant age-related changes specific for a certain genotype. Bonferroni post-hoc tests on the total SIPB number in SR showed a significant age-related reduction in SR of 10-month-old APP^{SL}/PS1ho KI mice compared to 2-month-old animals (−22.6%, p = 0.012; Figures 3C, 5). Although the mean total SIPB number in SR of 6-month-old APP^{SL}/PS1ho KI mice was at the same level as in SR of 10-month-old APP^{SL}/PS1ho KI mice (Figure 6A), post-hoc tests on age-related changes of total

SIPB numbers in SR between 6-month-old and 2-month-old APP^{SL}/PS1ho KI mice did not reach statistical significance ($p = 0.075$). Means and standard errors of SIPB densities and uncorrected SIPB numbers are given in Figure 7.

3.6 Age-related increases in SIPB-toneuron ratio in CA1–2 of APP^{SL}/PS1ho KI mice

Analyses of SIPB-to-neuron ratio focused on those regions and groups of mice showing age-related altered numbers of neurons and SIPB, namely the DG of PS1ho KI mice and the CA1–2 of APP^{SL}/PS1ho KI mice. In these groups, the mean SIPB-toneuron ratio in the CA1–2 of 10-month-old APP^{SL}/PS1ho KI mice was 50.6% higher compared to 2-month-old animals, ($p = 0.006$; Figure 3I), and 70.2% higher compared to 6-month-old animals ($p < 0.001$; Figure 6C). In contrast, the mean SIPB-to-neuron ratio in the DG of PS1ho KI mice did not differ between 10-month-old and 2-month-old animals (Figure 3G).

4. Discussion

4.1 Summary of results

The aims of the present study were to test the hypothesis that APP^{SL}/PS1ho KI mice show extensive loss of neurons and SIPB, whereas APP^{SL} and PS1ho KI mice do not, and to assess the relationships between neuron loss, synapse loss, extracellular Aβ aggregates, and intraneuronal Aβ in DG, CA3, and CA1–2. We show that APP^{SL}/PS1ho KI mice, but neither APP^{SL} mice nor PS1ho KI mice alone, are characterized by a marked age-related, region-specific neuron and synapse loss specifically in the CA1–2 between 2 and 10 months of age (Figures 4, 5). The loss of neurons within the CA1–2 coincided and surpassed SIPB loss within the same region, while intraneuronal accumulation of Aβ preceded both events [19]. Ultimately, the pathologic outcome is likely to be reflected by functional changes of the Schaffer collaterals that are highly layer-specific in the CA1 field. These afferent fibers may respond by degeneration, retraction, abnormal sprouting, or changes in targets within the area they normally innervate, resulting in alterations in synaptic function and plasticity. Furthermore, both SIPB and neuron loss greatly exceeded the local presence of extracellular Aβ aggregations (as shown by calculating reconstructed total neuron numbers and corrected SIPB numbers). These findings indicate that the synergistic action of both human mutant APP and mutant PS1 in CA1–2 heralded substantial loss of neurons and SIPB and that synaptic remodeling, reflected by an increased SIPB-to-neuron ratio, occurred concomitantly. In contrast to the neuron loss found in the APP^{SL}/PS1ho KI mice, a marked increase in neuron numbers was observed in the DG of PS1ho KI mice, which hints at an involvement of PS1 in neurogenesis.

4.2 Strengths and limitations of the study

Reduction of synaptophysin immunoreactivity in the hippocampus was found to be an early marker in human AD [27]. Furthermore, a loss of synapses is one of the prime correlates with cognitive decline and the duration of dementia in AD patients [28,29]. The relation between synapse loss and the classical neuropathological hallmarks, such as Aβ plaques and neurofibrillary tangles, has not been fully elucidated [30]. Exploring this relationship is pivotal, as it might prove to be an important link in the chain connecting the molecular pathology and clinical symptoms of AD, opening up new avenues for treatment strategies.

The present study is the first high-precision, quantitative neuroanatomical study focusing on age-related effects of human mutant APP and mutant PS1 on the numbers of neurons and synapses, and levels of Aβ in hippocampal subregions of mouse brains. The use of knock-in human PS1 into the mouse genome (under the mouse PS1 promoter) enhanced the biological validity of the study. The design and results have been validated in our previous reports [11,15].

Our study however has some limitations. First, the low number of mice in certain groups (particularly 6-month-old mice) may have decreased the statistical power of finding significant results across the three age groups of 2, 6, and 10-month-old mice. Directly linked to this, another limitation is our inability to calculate the indirect effect of gender on calculated parameters. Generalized linear model univariate analysis of variance allowed us to detect genotype and age effect, but could not generate a value for sex effect. Lastly, our quantitative analyses of SIPB numbers and SIPB-to-neuron ratios are not free of bias because SIPB densities were analyzed in one focal plane and thus in two instead of three dimensions. As we found similar distributions for individual SIPB sizes among groups and independence of the average SIPB size from the plane of section, it is reasonable to state that this limitation had no substantial impact on the results.

4.3 Age-related loss of neurons and SIPB in CA1–2 of APP^{SL}/PS1ho KI mice

Age-related loss of neurons and SIPB was restricted to the CA1–2 region of APP^{SL}/PS1ho KI mice. Thus, neither the neuronal presence of mutant APP found in the DG and in CA3 of APP^{SL}/PS1ho KI mice [19,31], nor the sole presence of mutant PS1 expressed at physiological levels by all cells in the brain of the PS1ho KI mice [19] was related to a substantial hippocampal neuron and synapse loss. As intraneuronal Aβ accumulation was apparent from 2 months of age in these mice, and occurred selectively in the CA1–2 of APP^{SL}/PS1ho KI mice, but neither in APP^{SL} nor in PS1ho KI mice (also shown in [19,22]), the observed age-related loss of neurons and synapses in the APP^{SL}/PS1ho KI mice is consistent with a causative involvement of an intraneuronal Aβ species. In agreement with our findings, it was observed recently that intraneuronal accumulation of different Aβ peptides between 2 and 6 months of age, together with overall accumulation of N-modified, fibrillar and oligomeric species coincided well with drastic reduction of synaptic plasticity of CA1–2 neurons in our APP^{SL}/PS1ho KI mouse model [32]. A similar relationship between intracellular Aβ species and synaptic pathology was also reported in $APP_{E693}\Delta$-Tg mice [33] and $PS1^{M146L}/APP751^{SL}$ mice [34]. These findings, together with the present data, suggest a key role of Aβ at the synapse, underscoring the role of prefibrillar Aβ oligomers, including intraneuronal Aβ, in AD pathogenesis. Although both human mutant APP and mutant PS1 were expressed in the DG, we did not observe levels of Aβ detectable with immunohistochemistry in the DG of APP^{SL}/PS1ho KI mice at 2 and 10 months of age. The reasons for this lack of detectable Aβ (despite coexpression of mutant APP as well as mutant PS1) are currently unknown but may involve decreased production, decreased accumulation, enhanced degradation, or enhanced removal of Aβ in the DG.

Other studies using mouse models with overexpression of familial AD-linked APP and PS1 mutations did not demonstrate either intraneuronal Aβ deposition or considerable neuron

and synapse loss by quantitative counting methods [35–40]. Breyhan and colleagues demonstrated a 33% pyramidal cell loss within the CA1–2 in 6-month-old APP^{SL}/PS1ho KI mice (*i.e.*, the same mouse strain as the one used in the present study) together with a drastic reduction of LTP and disrupted paired-pulse facilitation [32]. These data suggest that feedback inhibition in the DG and feedforward inhibition in CA3 are likely to be impaired as well, in turn leading to hyperexcitability of the hippocampal circuits, and transfer of abnormal activity in the affected CA1–2 region. Conceptually, this provides a novel means by which hippocampal excitability can be increased, which will require further electrophysiologic characterization. Reduced LTP in these mice was corroborated by strongly decreased levels of pre- (clathrin light chain, SNAP25) and postsynaptic markers (PSD-95) in synaptosome fractions. In addition, pyroglutamate N3(pE)-modified Aβ species displayed as much as a 435% increased acceleration of the initial formation of Aβ aggregates in CA1–2 neurons [32]. It should be noted that Breyhan and colleagues focused on neuron and synaptic dysfunction or loss by comparing APP^{SL}/PS1ho KI mice to PS1ho KI mice, and did not analyze age-related changes in total numbers of neurons or SIPB. Furthermore, Western blot analyses of synaptic proteins were carried out on tissue homogenates, which lack regional and cell-type-specific resolutions. Based on these considerations, the findings of Breyhan and colleagues [32] cannot be compared directly with ours.

Cotel and colleagues [31] showed that APP^{SL}/PS1ho KI mice displayed a 48% loss of DG granule cells as compared to 12-month-old female PS1ho KI mice. This seems to contrast our findings of no significant age-related neuron loss between 2 and 10 months of age in the DG in APP^{SL}/PS1ho KI mice as compared to APP^{SL} mice and PS1ho KI mice. Although it may be possible that substantial loss of DG granule cells occurs between 10 and 12 months of age, or that the neurodegenerative effects primarily affect female mice, altered neurogenesis in PS1ho KI and APP^{SL}/PS1ho KI mice may also account for some of the differences. For example, mixed results on cytogenesis and neurogenesis have been found for effects of expressing human mutant APP and PS1 constructs in mice [41] and neurogenesis has not yet been assessed in APP^{SL}/PS1ho KI mice. Although the present study has the advantages of assessing age-related changes by comparing 10 versus 2-month-old mice, measuring total numbers of neuron and SIPB with highprecision methodologies in a hippocampal subregion-specific manner, and including APP^{SL} mice in the analyses, it remains to be determined whether drastic neuron loss occurs in the DG in APP^{SL}/PS1ho KI mice between 10 and 12 months of age, or that knock-in of PS1 enhances genesis, neuronal differentiation or survival of progenitor cells in DG and thereby accounting for the preserved total neuron numbers in DG of 10-month-old APP^{SL}/PS1ho KI mice.

4.4 Age-related increase in SIPB-to-neuron ratio in APP^{SL}/PS1ho KI mice

Our finding of a 50.6% and 70.2% percent increase in the SIPB-to-neuron ratio in 10-month-old APP^{SL}/PS1ho KI mice compared to 2- and 6-month-old mice respectively, may indicate the occurrence of synaptic remodeling and synaptic plasticity. As the increase in SIPB-to-neuron ratio was only apparent between 10-month-old mice and 6-month-old mice rather than 6-month-old mice and 2-month-old mice, compensatory synaptic remodeling may only have been activated after substantial neurodegeneration. Similar observations have

been observed for synaptophysin and other presynaptic proteins in neocortical association areas at Braak stage III of AD progression, prior to neurofibrillary pathology [42], for drebrin in the prefrontal cortex of patients with mild cognitive impairment followed by 40–60% decrease in severe AD [43], as well as for glutamatergic presynaptic bouton density in midfrontal gyrus of mild cognitive impairment patients [44], but not for total numbers of spinophilin-immunoreactive puncta in the CA1 and CA3 fields of hippocampus and area 9 in elderly individuals with various degrees of cognitive decline [45]. Moreover, Bronfman et al. [46] described a “synaptic sprouting compensatory mechanism” in the hippocampus of aged PDAPP mice exhibiting atrophied cholinergic neurons in the medial septum. Finding of compensatory mechanism associated with a greater SIPB-to-neuron ratio in aged transgenic mice is not unique; similar results have been obtained for the synapse-to-granule cell ratio following behavioral training and cerebral ischemia [47]. This could of course result in subtle changes in neuronal connectivity, which, in turn, could affect normal brain function.

4.5 No age-related loss of SIPB numbers in APP^{SL} mice and PS1ho KI mice

Our data demonstrate that aging, at least up to 10 months of age, had a general effect on SIPB numbers, without particularly decreasing SIPB numbers in APP^{SL} mice and PS1ho KI mice. Although findings of reduced synaptophysin immunoreactivity and synaptic densities in hippocampus of AD patients have been consistent [48], the effects on synaptic degeneration by APP and/or PS1 transgenes, Aβ production, and Aβ deposition vary among different transgenic mouse lines [12–16, 49]. Our finding that the APP^{SL} transgene did not affect SIPB densities or SIPB numbers, along with unchanged total numbers of neurons, in the DG, CA3, and CA1–2 agrees with our previous findings on 4.5-month-old, single transgenic APP^{SL} mice using the same methodologies [15] and with findings from other groups [12,35,50].

Similarly, our analyses show that SIPB numbers in SM, SL, and SR were not significantly altered in PS1ho KI mice, despite increased number of granule cells in the DG during aging. The preservation of SIPB numbers in hippocampus of PS1ho KI mice during aging is in agreement with other studies using transgenic mice that overexpress PS1 M146L or P264L mutations [15,37,51,52]. From the functional point of view, PS1 mutations alone may induce abnormalities in synaptic transmission [53], calcium homeostasis [54], and fast axonal transport [55]. However, findings from our previous study on 17-month-old PS1 M146L mice suggest that mutant PS1 may have structural effects in a region-specific manner at a later age [15]. The varying reports on synaptic changes reported for transgenic mouse models of AD, based either on the overexpression of mutant human APP or mutant form of PS1, may in part be explained by: (i) discrepancy between functional and structural abnormalities; (ii) variable degrees of balance between trophic effects of APP or PS1 on synapses and the toxic effects of Aβ and its derivatives; (iii) different handling, trafficking and signaling properties among diverse mutations in APP or PS1 and/or the used promoters; (iv) compensatory changes in synaptic morphology; (v) differences in the methods used to quantify numbers or densities of presynaptic boutons; or (vi) differences in ages and genetic backgrounds of investigated mouse strains. Additional studies are needed to test these mechanisms directly using both animal and human samples.

4.6 Age-related increase in neuron number in DG of PS1ho KI mice

Our results indicated an increase of approximately 38% in the total number of neurons in the DG of 10-month-old PS1ho KI mice as compared to 2-month-old PS1ho KI mice. These results are in line with our previous findings of an age-related increase in total number of neurons in layers II to IV of the frontal cortex, particularly parvalbumin-immunoreactive neurons, in the same mice [57] and supports further evidence in the literature suggesting a role for of PS1 in neurogenesis [56–58].

In conclusion, the APP^{SL}/PS1ho KI mouse model as investigated in our study provides a model to investigate hippocampal region-specific differences in interactions between altered APP and PS1, the consequent production and accumulation of various Aβ species, and their spatial and temporal relations with loss of neurons, altered synaptic connections, neuroplasticity, and neurogenesis.

Acknowledgments

We thank Drs. V. Blanchard-Bregeon and L. Pradier for providing the transgenic animals, Dr. G. Multhaup for providing rabbit anti-mouse polyclonal antiserum 730, Dr. D. Hopkins for critically reading of the manuscript, and Mrs. H.P.J. Steinbusch for expert technical assistance. This work was supported in part by NIH grant AG05138 (to D.L.D. and P.R.H.), the Internationale Stichting Alzheimer Onderzoek (ISAO) grant number 09552, and the Netherlands Organisation for Scientific Research (NWO) Veni Award 916.11.086 to B.P.F.R.

Abbreviations

Aβ	amyloid beta protein
AD	Alzheimer’s disease
APP	amyloid precursor protein
DG	dentate gyrus
GFAP	glial fibrillary acidic protein
KI	knock-in
LTP	long-term potentiation
M2	2-month-old
M10	10-month-old
PS1	presenilin 1
SIPB	synaptophysin-immunoreactive presynaptic boutons
SL	*stratum lucidum*
SM	*stratum moleculare*
SR	*stratum radiatum*
TBS	Tris-buffered saline

References

1. Scheff SW, Price DA, Schmitt FA, Scheff MA, Mufson EJ. Synaptic loss in the inferior temporal gyrus in mild cognitive impairment and Alzheimer's disease. J. Alzheimers Dis. 2011; 24:547–557. [PubMed: 21297265]
2. Selkoe DJ. Alzheimer's disease is a synaptic failure. Science. 2002; 298:789–791. [PubMed: 12399581]
3. Walsh DM, Selkoe DJ. Deciphering the molecular basis of memory failure in Alzheimer's disease. Neuron. 2004; 44:181–193. [PubMed: 15450169]
4. Yu W, Lu B. Synapses and dendritic spines as pathogenic targets in Alzheimer's disease. Neural Plast. 2012; 2012:1–8.
5. Tam JH, Pasternak SH. Amyloid and Alzheimer's disease: inside and out. Can. J. Neurol. Sci. 2012; 39:286–298. [PubMed: 22547507]
6. Luque FA, Jaffe SL. The molecular and cellular pathogenesis of dementia of the Alzheimer's type an overview. Int. Rev. Neurobiol. 2009; 84:151–165. [PubMed: 19501717]
7. Fjell AM, Walhovd KB. Neuroimaging results impose new views on Alzheimer's disease—the role of amyloid revised. Mol. Neurobiol. 2012:1–20.
8. Hardy J, Selkoe DJ. The amyloid hypothesis of Alzheimer's disease: progress and problems on the road to therapeutics. Science. 2002; 297:353–356. [PubMed: 12130773]
9. Mucke L, Masliah E, Yu GQ, Mallory M, Rockenstein EM, Tatsuno G, et al. High-level neuronal expression of abeta 1–42 in wild-type human amyloid protein precursor transgenic mice: synaptotoxicity without plaque formation. J. Neurosci. 2000; 20:4050–4058. [PubMed: 10818140]
10. Klein WL, Krafft GA, Finch CE. Targeting small Abeta oligomers: the solution to an Alzheimer's disease conundrum? Trends Neurosci. 2001; 24:219–224. [PubMed: 11250006]
11. Schmitz C, Rutten BP, Pielen A, Schafer S, Wirths O, Tremp G, et al. Hippocampal neuron loss exceeds amyloid plaque load in a transgenic mouse model of Alzheimer's disease. Am. J. Pathol. 2004; 164:1495–1502. [PubMed: 15039236]
12. Boncristiano S, Calhoun ME, Howard V, Bondolfi L, Kaeser SA, Wiederhold KH, et al. Neocortical synaptic bouton number is maintained despite robust amyloid deposition in APP23 transgenic mice. Neurobiol. Aging. 2005; 26:607–613. [PubMed: 15708435]
13. Dickey CA, Loring JF, Montgomery J, Gordon MN, Eastman PS, Morgan D. Selectively reduced expression of synaptic plasticity-related genes in amyloid precursor protein + presenilin-1 transgenic mice. J. Neurosci. 2003; 23:5219–5226. [PubMed: 12832546]
14. Hsia AY, Masliah E, McConlogue L, Yu GQ, Tatsuno G, Hu K, et al. Plaque-independent disruption of neural circuits in Alzheimer's disease mouse models. Proc. Natl. Acad. Sci. USA. 1999; 96:3228–3233. [PubMed: 10077666]
15. Rutten BP, Van der Kolk NM, Schafer S, van Zandvoort MA, Bayer TA, Steinbusch HW, et al. Age-related loss of synaptophysin immunoreactive presynaptic boutons within the hippocampus of APP751SL, PS1M146L, and APP751SL/PS1M146L transgenic mice. Am. J. Pathol. 2005; 167:161–173. [PubMed: 15972962]
16. West MJ, Bach G, Soderman A, Jensen JL. Synaptic contact number and size in stratum radiatum CA1 of APP/PS1DeltaE9 transgenic mice. Neurobiol. Aging. 2009; 30:1756–1776. [PubMed: 18336954]
17. Nizzari M, Thellung S, Corsaro A, Villa V, Pagano A, Porcile C, et al. Neurodegeneration in Alzheimer disease: role of amyloid precursor protein and presenilin 1 intracellular signaling. J. Toxicol. 2012; 2012:1–13.
18. Revett TJ, Baker GB, Jhamandas J, Kar S. Glutamate system, amyloid β peptides and tau protein: functional interrelationships and relevance to Alzheimer disease pathology. J. Psychiatry Neurosci. 2013; 38:6–23. [PubMed: 22894822]
19. Casas C, Sergeant N, Itier JM, Blanchard V, Wirths O, van der Kolk N, et al. Massive CA1/2 neuronal loss with intraneuronal and N-terminal truncated Abeta42 accumulation in a novel Alzheimer transgenic model. Am. J. Pathol. 2004; 165:1289–1300. [PubMed: 15466394]

20. Wirths O, Breyhan H, Schafer S, Roth C, Bayer TA. Deficits in working memory and motor performance in the APP/PS1ki mouse model for Alzheimer's disease. Neurobiol. Aging. 2008; 29:891–901. [PubMed: 17215062]
21. Wirths O, Weis J, Szczygielski J, Multhaup G, Bayer TA. Axonopathy in an APP/PS1 transgenic mouse model of Alzheimer's disease. Acta Neuropathol. 2006; 111:312–319. [PubMed: 16520967]
22. Takahashi H, Brasnjevic I, Rutten BP, Van Der Kolk N, Perl DP, Bouras C, et al. Hippocampal interneuron loss in an APP/PS1 double mutant mouse and in Alzheimer's disease. Brain Struct. Funct. 2010; 214:145–160. [PubMed: 20213270]
23. Borchardt T, Camakaris J, Cappai R, Masters CL, Beyreuther K, Multhaup G. Copper inhibits beta-amyloid production and stimulates the non-amyloidogenic pathway of amyloid-precursor-protein secretion. Biochem. J. 1999; 344:461–467. [PubMed: 10567229]
24. Schmitz C, Hof PR. Design-based stereology in neuroscience. Neuroscience. 2005; 130:813–831. [PubMed: 15652981]
25. Franklin, K.; Paxinos, G. The mouse brain in stereotaxic coordinates. San Diego: Academic Press; 1997.
26. Van de Berg WD, Blokland A, Cuello AC, Schmitz C, Vreuls W, Steinbusch HW, et al. Perinatal asphyxia results in changes in presynaptic bouton number in striatum and cerebral cortex-a stereological and behavioral analysis. J. Chem. Neuroanat. 2000; 20:71–82. [PubMed: 11074345]
27. Heinonen O, Soininen H, Sorvari H, Kosunen O, Paljarvi L, Koivisto E, et al. Loss of synaptophysin-like immunoreactivity in the hippocampal formation is an early phenomenon in Alzheimer's disease. Neuroscience. 1995; 64:375–385. [PubMed: 7700527]
28. Terry RD, Masliah E, Salmon DP, Butters N, DeTeresa R, Hill R, et al. Physical basis of cognitive alterations in Alzheimer's disease: synapse loss is the major correlate of cognitive impairment. Ann. Neurol. 1991; 30:572–580. [PubMed: 1789684]
29. Ingelsson M, Fukumoto H, Newell KL, Growdon JH, Hedley-Whyte ET, Frosch MP, et al. Early Aβ accumulation and progressive synaptic loss, gliosis, and tangle formation in AD brain. Neurology. 2004; 62:925–931. [PubMed: 15037694]
30. Clare R, King VG, Wirenfeldt M, Vinters HV. Synapse loss in dementias. J. Neurosci. Res. 2010; 88:2083–2090. [PubMed: 20533377]
31. Cotel MC, Bayer TA, Wirths O. Age-dependent loss of dentate gyrus granule cells in APP/PS1KI mice. Brain Res. 2008; 1222:207–213. [PubMed: 18585693]
32. Breyhan H, Wirths O, Duan K, Marcello A, Rettig J, Bayer TA. APP/PS1KI bigenic mice develop early synaptic deficits and hippocampus atrophy. Acta Neuropathol. 2009; 117:677–685. [PubMed: 19387667]
33. Tomiyama T, Matsuyama S, Iso H, Umeda T, Takuma H, Ohnishi K, et al. A mouse model of amyloid β oligomers: their contribution to synaptic alteration, abnormal tau phosphorylation, glial activation, and neuronal loss in vivo. J. Neurosci. 2010; 30:4845–4856. [PubMed: 20371804]
34. Sanchez-Varo R, Trujillo-Estrada L, Sanchez-Mejias E, Torres M, Baglietto-Vargas D, Moreno-Gonzalez I, et al. Abnormal accumulation of autophagic vesicles correlates with axonal and synaptic pathology in young Alzheimer's mice hippocampus. Acta Neuropathol. 2012:1–18.
35. Irizarry MC, Soriano F, McNamara M, Page KJ, Schenk D, Games D, et al. Abeta deposition is associated with neuropil changes, but not with overt neuronal loss in the human amyloid precursor protein V717F (PDAPP) transgenic mouse. J. Neurosci. 1997; 17:7053–7059. [PubMed: 9278541]
36. Calhoun ME, Wiederhold KH, Abramowski D, Phinney AL, Probst A, Sturchler-Pierrat C, et al. Neuron loss in APP transgenic mice. Nature. 1998; 395:755–756. [PubMed: 9796810]
37. Takeuchi A, Irizarry MC, Duff K, Saido TC, Hsiao Ashe K, Hasegawa M, et al. Age-related amyloid beta deposition in transgenic mice overexpressing both Alzheimer mutant presenilin 1 and amyloid beta precursor protein Swedish mutant is not associated with global neuronal loss. Am. J. Pathol. 2000; 157:331–339. [PubMed: 10880403]
38. Dickson DW. Building a more perfect beast: APP transgenic mice with neuronal loss. Am. J. Pathol. 2004; 164:1143–1146. [PubMed: 15039203]

39. Howlett DR, Bowler K, Soden PE, Riddell D, Davis JB, Richardson JC, et al. Abeta deposition and related pathology in an APP × PS1 transgenic mouse model of Alzheimer's disease. Histol. Histopathol. 2008; 23:67–76. [PubMed: 17952859]
40. Van Broeck B, Vanhoutte G, Pirici D, Van Dam D, Wils H, Cuijt I, et al. Intraneuronal amyloid beta and reduced brain volume in a novel APP T714I mouse model for Alzheimer's disease. Neurobiol. Aging. 2008; 29:241–252. [PubMed: 17112635]
41. Elder GA, Gama Sosa MA, De Gasperi R, Dickstein DL, Hof PR. Presenilin transgenic mice as models of Alzheimer's disease. Brain Struct. Funct. 2010; 214:127–143. [PubMed: 19921519]
42. Mukaetova-Ladinska EB, Garcia-Siera F, Hurt J, Gertz HJ, Xuereb JH, Hills R, et al. Staging of cytoskeletal and beta-amyloid changes in human isocortex reveals biphasic synaptic protein response during progression of Alzheimer's disease. Am. J. Pathol. 2000; 157:623–636. [PubMed: 10934165]
43. Counts SE, Nadeem M, Lad SP, Wuu J, Mufson EJ. Differential expression of synaptic proteins in the frontal and temporal cortex of elderly subjects with mild cognitive impairment. J. Neuropathol. Exp. Neurol. 2006; 65:592–601. [PubMed: 16783169]
44. Bell KF, Bennett DA, Cuello AC. Paradoxical upregulation of glutamatergic presynaptic boutons during mild cognitive impairment. J. Neurosci. 2007; 27:10810–10817. [PubMed: 17913914]
45. Akram A, Christoffel D, Rocher AB, Bouras C, Kovari E, Perl DP, et al. Stereologic estimates of total spinophilin-immunoreactive spine number in area 9 and the CA1 field: relationship with the progression of Alzheimer's disease. Neurobiol. Aging. 2008; 29:1296–1307. [PubMed: 17420070]
46. Bronfman FC, Moechars D, Van Leuven F. Acetylcholinesterase-positive fiber deafferentation and cell shrinkage in the septohippocampal pathway of aged amyloid precursor protein london mutant transgenic mice. Neurobiol. Dis. 2000; 7:152–168. [PubMed: 10860782]
47. Briones TL, Suh E, Jozsa L, Rogozinska M, Woods J, Wadowska M. Changes in number of synapses and mitochondria in presynaptic terminals in the dentate gyrus following cerebral ischemia and rehabilitation training. Brain Res. 2005; 1033:51–57. [PubMed: 15680339]
48. DeKosky ST, Scheff SW, Styren SD. Structural correlates of cognition in dementia: quantification and assessment of synapse change. Neurodegeneration. 1996; 5:417–421. [PubMed: 9117556]
49. Seeger G, Gärtner U, Ueberham U, Rohn S, Arendt T. FAD-mutation of APP is associated with a loss of its synaptotrophic activity. Neurobiol. Dis. 2009; 35:258–263. [PubMed: 19450683]
50. Dong H, Martin MV, Chambers S, Csernansky JG. Spatial relationship between synapse loss and β-amyloid deposition in Tg2576 mice. J. Comp. Neurol. 2006; 500:311–321. [PubMed: 17111375]
51. Hu L, Wong TP, Cote SL, Bell KF, Cuello AC. The impact of Abeta-plaques on cortical cholinergic and non-cholinergic presynaptic boutons in alzheimer's disease-like transgenic mice. Neuroscience. 2003; 121:421–432. [PubMed: 14522000]
52. Savage MJ, Lin YG, Ciallella JR, Flood DG, Scott RW. Activation of c-Jun N-terminal kinase and p38 in an Alzheimer's disease model is associated with amyloid deposition. J. Neurosci. 2002; 22:3376–3385. [PubMed: 11978814]
53. Gruart A, Lopez-Ramos JC, Munoz MD, Delgado-Garcia JM. Aged wild-type and APP PS1, and APP + PS1 mice present similar deficits in associative learning and synaptic plasticity independent of amyloid load. Neurobiol. Dis. 2008; 30:439–450. [PubMed: 18442916]
54. Koo EH, Kopan R. Potential role of presenilin-regulated signaling pathways in sporadic neurodegeneration. Nat. Med. 2004; 10(Suppl.):S26–S33. [PubMed: 15272268]
55. Morfini G, Pigino G, Beffert U, Busciglio J, Brady ST. Fast axonal transport misregulation and Alzheimer's disease. Neuromolecular Med. 2002; 2:89–99. [PubMed: 12428805]
56. Gadadhar A, Marr R, Lazarov O. Presenilin-1 regulates neural progenitor cell differentiation in the adult brain. J. Neurosci. 2011; 31:2615–2623. [PubMed: 21325529]
57. Lemmens MAM, Sierksma ASR, Rutten BPF, Dennissen F, Steinbusch HWM, Lucassen PJ, et al. Age-related changes of neuron numbers in the frontal cortex of a transgenic mouse model of Alzheimer's disease. Brain Struct. Funct. 2011; 216:227–237. [PubMed: 21409417]
58. van Tijn P, Kamphuis W, Marlatt MW, Hol EM, Lucassen PJ. Presenilin mouse and zebrafish models for dementia: focus on neurogenesis. Prog. Neurobiol. 2011; 93:149–164. [PubMed: 21056616]

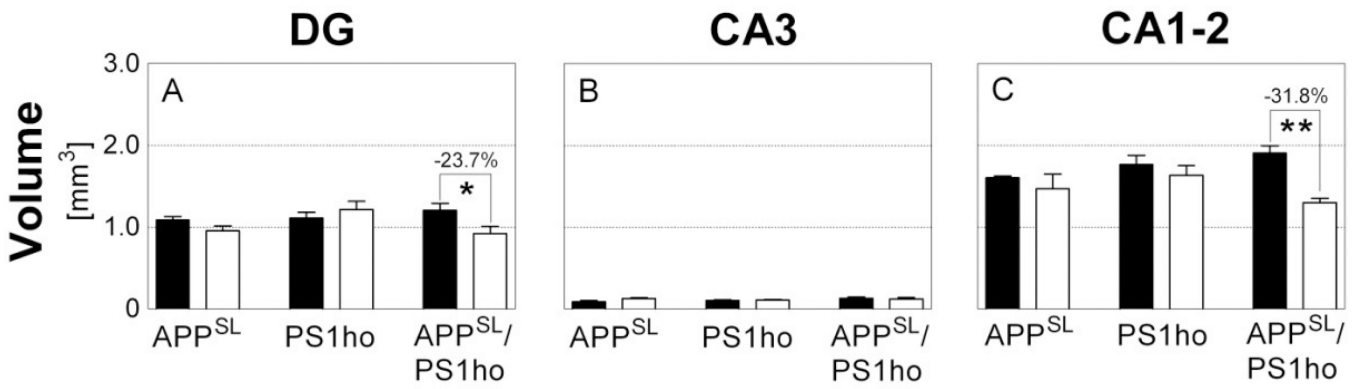

Figure 1.

Mean and standard error of the mean of estimated volumes in the *stratum moleculare* of the dentate gyrus (A; DG), *stratum lucidum* of area CA3 (B; CA3) and *stratum radiatum* of area CA1–2 (C; CA1–2) in the hippocampus of 2-month-old (M2; black bars) and 10-month-old (M10; open bars) APP^{SL} mice (APP^{SL}), PS1ho KI mice (PS1ho) and APP^{SL}/PS1ho KI mice (APP^{SL}/PS1ho). Results of general linear model univariate analysis of variance are summarized in Table 1; results of post-hoc Bonferroni tests for pairwise comparisons between animals in groups M2 and M10 of the same genotype are indicated in the graphs. *, $p < 0.05$; **, $p < 0.01$.

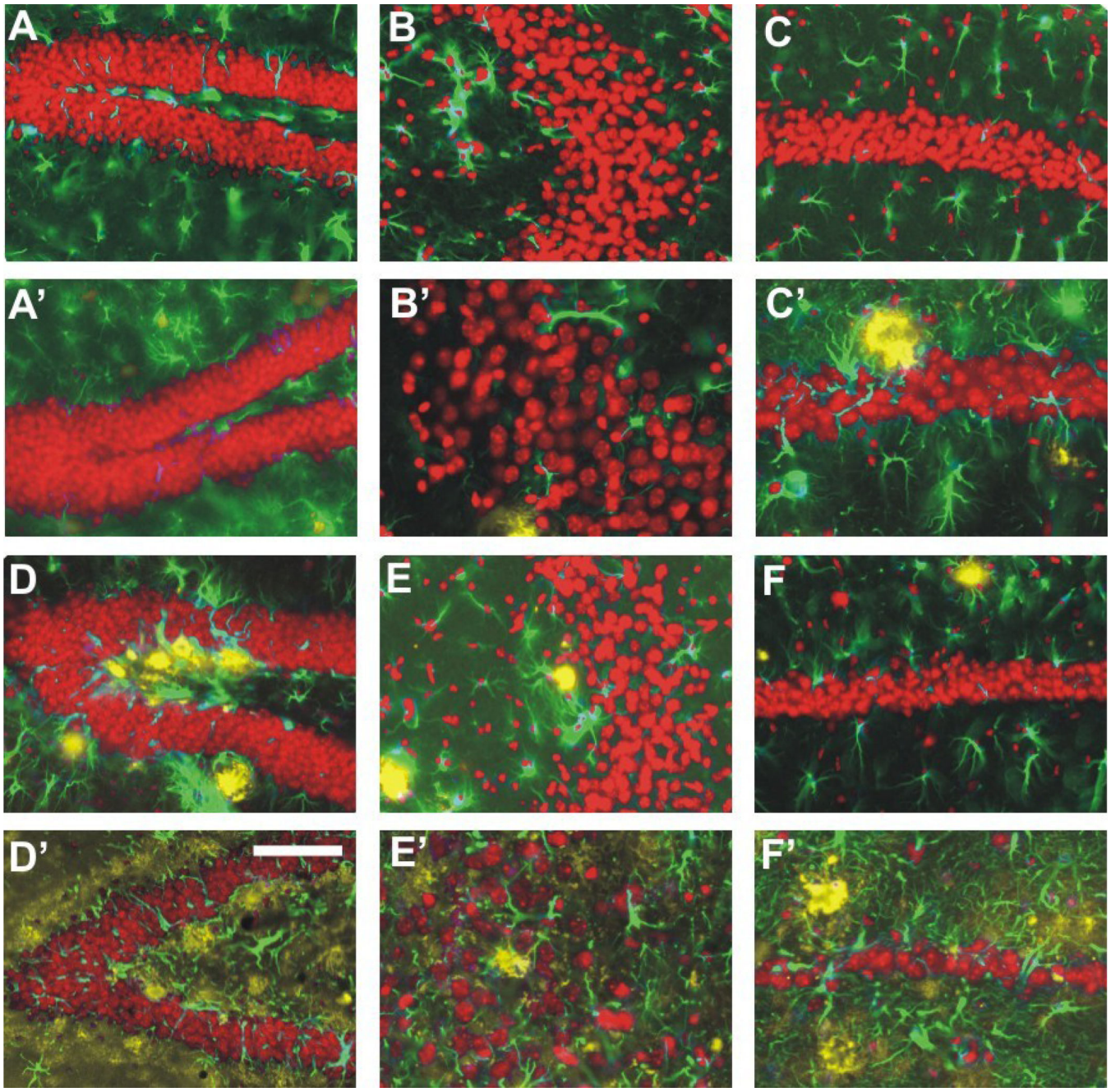

Figure 2.

Representative high-power photomicrographs showing region-specific immunofluorescence detection of Aβ (yellow fluorescence) and GFAP (green fluorescence) within the dentate gyrus (A, A', D, D'), CA3 (B, B', E, E') and CA1–2 (C, C', F, F') in the hippocampus of APP^{SL} mice at 2 month of age (M2; A to C) and 10 months of age (M10; A' to C') as well as of APP^{SL}/PS1ho KI mice at M2 (D to F) and M10 (D' to F') (sections counterstained with Hoechst 33342, pseudocolored in red for better contrast). Note the age-related aggregation of extracellular Aβ, the strong increase in GFAP immunoreactivity and

particularly the neuron within the CA1–2 of the APP^{SL}/PS1ho KI mice. Scale bar = 33 μm in A, A', B, B', D, D', E and E', and 50 μm in C, C', F and F'.

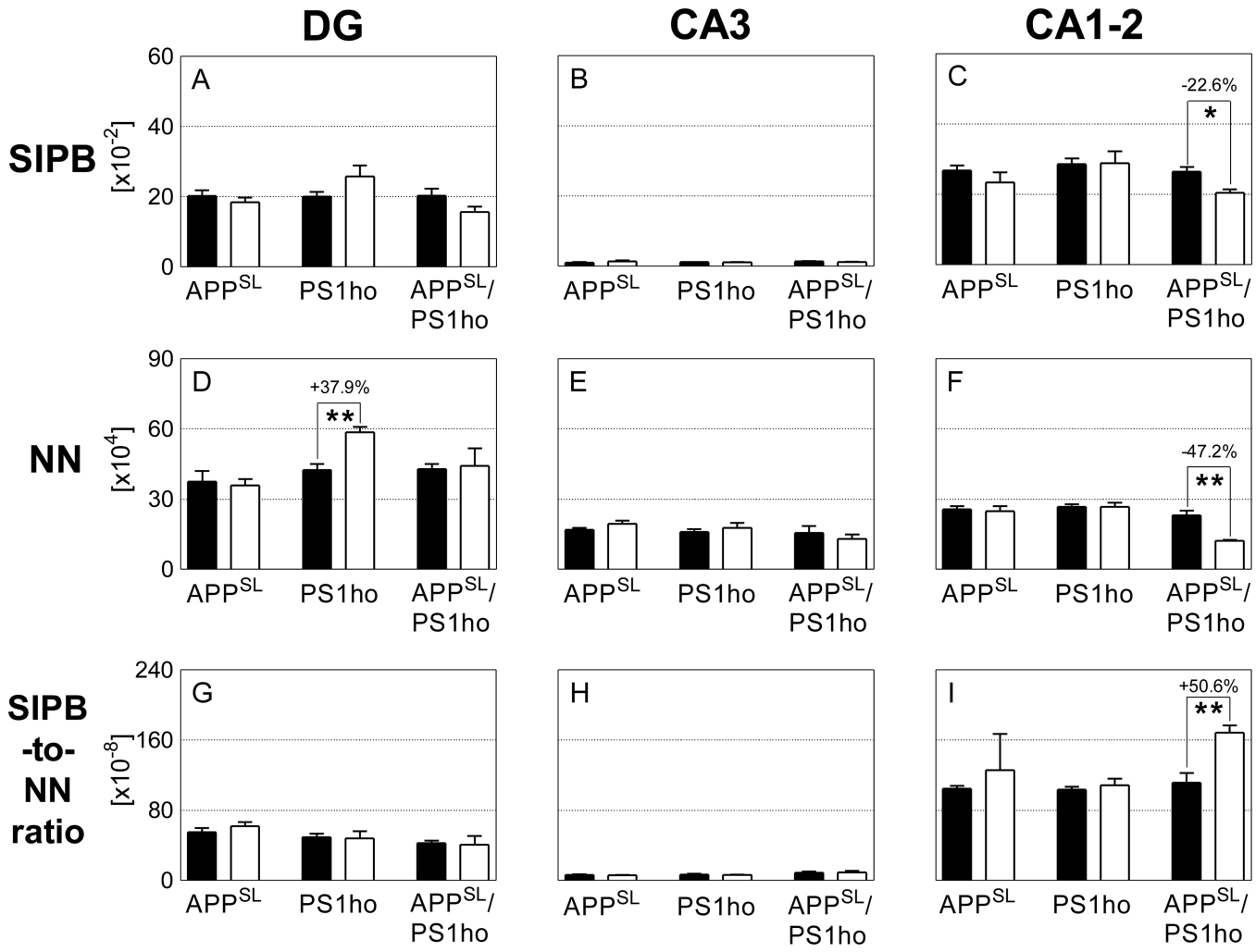

Figure 3.

Mean and standard error of the mean of total number of synaptophysin-immunoreactive presynaptic boutons (A–C; SIPB), total neuron numbers (D–F; NN) and SIPB-to-neuron number ratio (G–I; SIPB-to-NN) in the DG (A, D, G), CA3 (B, E, H), and CA1–2 (C, F, I) in the hippocampus of either 2-month-old (M2; black bars) or 10-month-old (M10; open bars) APP^{SL} mice (APP^{SL}), PS1ho KI mice (PS1ho) and APP^{SL}/PS1ho KI mice (APP^{SL}/PS1ho). Results of general linear model univariate analysis of variance are summarized in Table 2; results of post-hoc Bonferroni tests for pairwise comparisons between animals in groups M2 and M10 of the same genotype are indicated in the graphs. *, $p < 0.05$; **, $p < 0.01$.

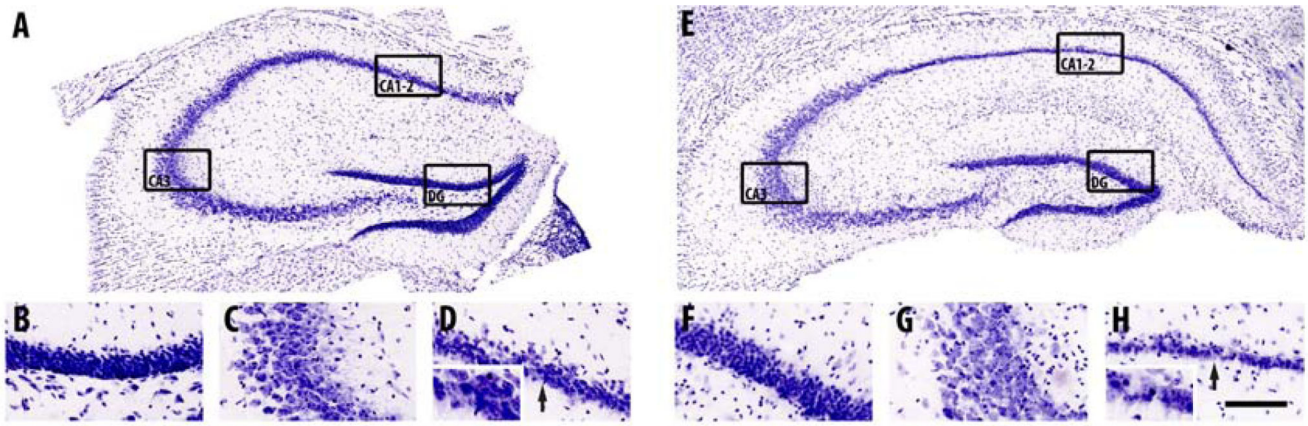

Figure 4.

Representative images of Nissl staining in the hippocampus (A), dentate gyrus (DG; B), CA3 region (C) and CA1–2 region (D) of a 2-month-old APP^{SL}/PS1ho KI mouse, and in the hippocampus (E), dentate gyrus (F), CA3 region (G) and CA1–2 region (H) of a 10-month-old APP^{SL}/PS1ho KI mouse. Note the specific loss of CA1–2 neurons in the 10-month-old mouse (E, H, insert H), as compared to the 2-month-old mouse (A, D, insert D), and as indicated by the black arrows. The black rectangles indicate the areas where B–D and F–H correspond to in A and E, respectively. The scale bar represents 1400 μm in A and E, 448 μm in B–D and F–H, and 224 μm in the inserts of D and H.

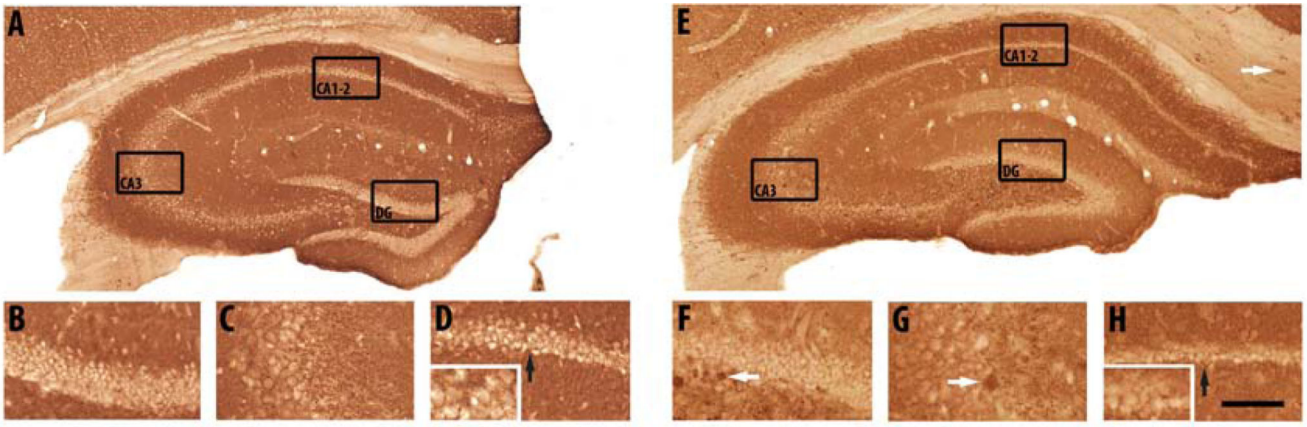

Figure 5.

Representative images of synaptophysin immunoreactivity in the hippocampus (A), dentate gyrus (DG; B), CA3 region (C) and CA1–2 region (D) of a 2-month-old APP^{SL}/PS1ho KI mouse, and in the hippocampus (E), dentate gyrus (F), CA3 region (G) and CA1–2 region (H) of a 10-month-old APP^{SL}/PS1ho KI mouse. The white arrows (E, F, G) indicate possible dystrophic neurites, which have high synaptophysin immunoreactivity. Note the specific loss of CA1–2 neurons in the 10-month-old mouse (E, H, insert H), as compared to the 2 month old mouse (A, D, insert H), and as indicated by the black arrows. The black rectangles indicate the areas where B–D and F–H correspond to in A and E, respectively. The scale bar represents 1400 μm in A and E, 448 μm in B–D and F–H, and 224 μm in the inserts of D and H.

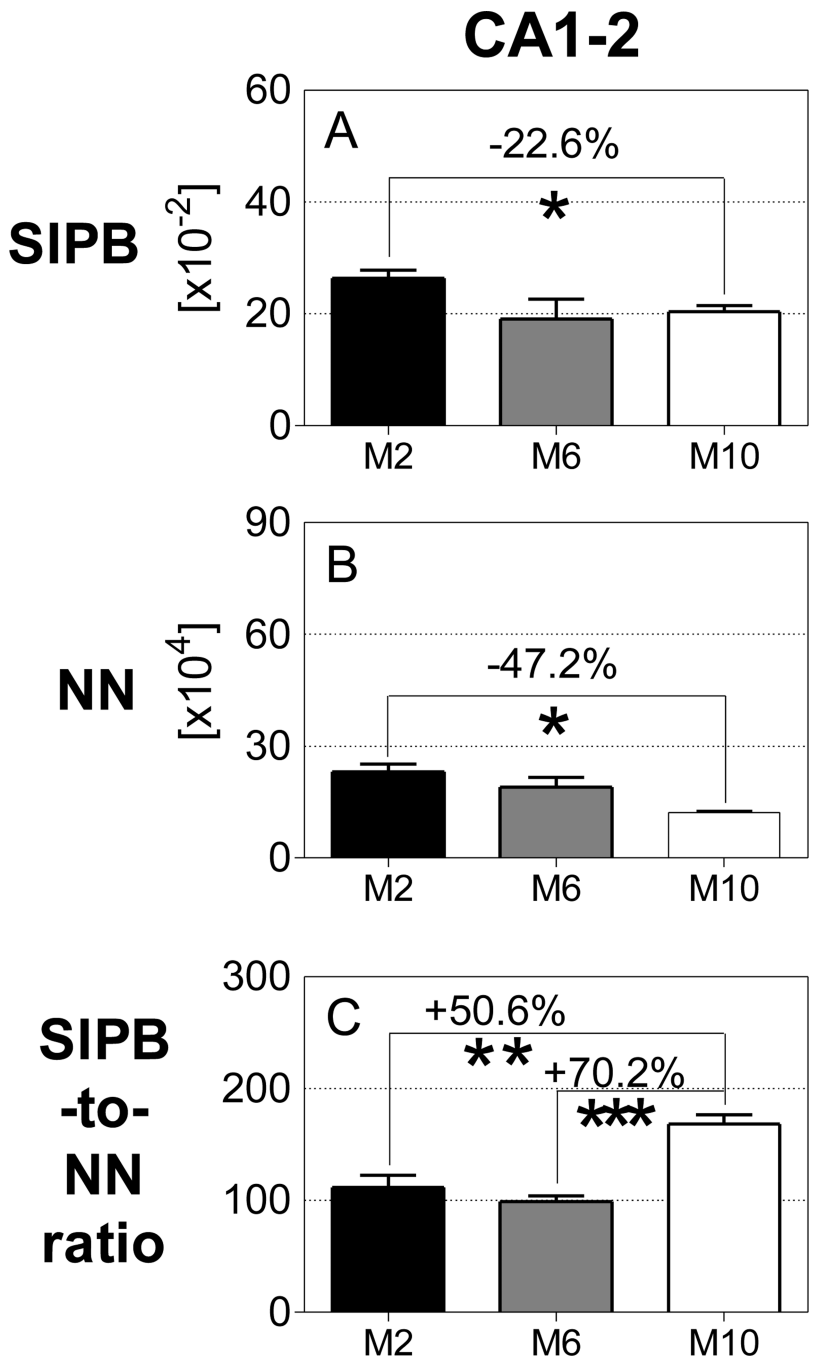

Figure 6.

Mean and standard error of the mean of total number of synaptophysin-immunoreactive presynaptic boutons numbers (A; SIPB), total number of neurons (B; NN) and SIPB-to-neuron number ratio (C; SIPB-to-NN ratio) in the CA1–2 of 2-month-old (M2; black bars), 6-month-old (M6; dark grey bars) or 10-month-old (M10; open bars) APP^{SL}/PS1ho KI mice. Results of post-hoc Bonferroni tests for pairwise comparisons between animals in groups M2 and M6, M6 and M10 and M2 and M10 of the same genotype are indicated in the graphs. *, $p < 0.05$; **, $p < 0.01$.

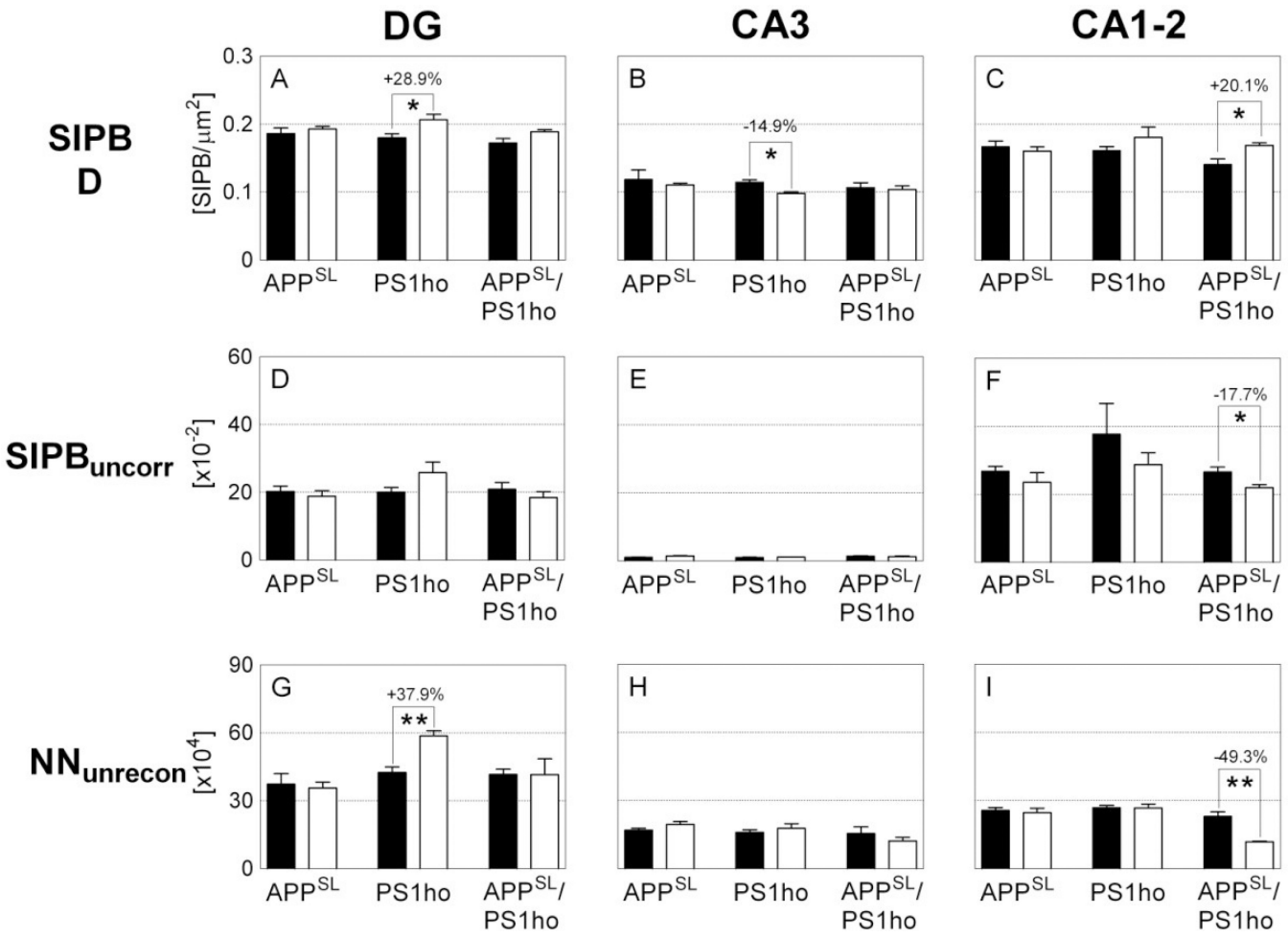

Figure 7.

Mean and standard error of the mean of synaptophysin-immunoreactive presynaptic boutons (SIPB) densities (A–C; SIPB D), uncorrected SIPB numbers (D–F; $SIPB_{uncorr}$) and unreconstructed total neuron numbers (G–I; $NN_{unrecon}$) in the DG (A, D,G), CA3 (B, E, H), and CA1–2 (C, F, I) in the hippocampus of either 2-month-old (M2; black bars) or 10-month-old (M10; open bars) APP^{SL} mice (APP^{SL}), PS1ho KI mice (PS1ho) and APP^{SL}/PS1ho KI mice (APP^{SL}/PS1ho). Results of post-hoc Bonferroni tests for pairwise comparisons between animals in groups M2 and M10 of the same genotype (after general linear model univariate analyses of variance was performed) are indicated in the graphs. *, $p < 0.05$; **, $p < 0.01$.

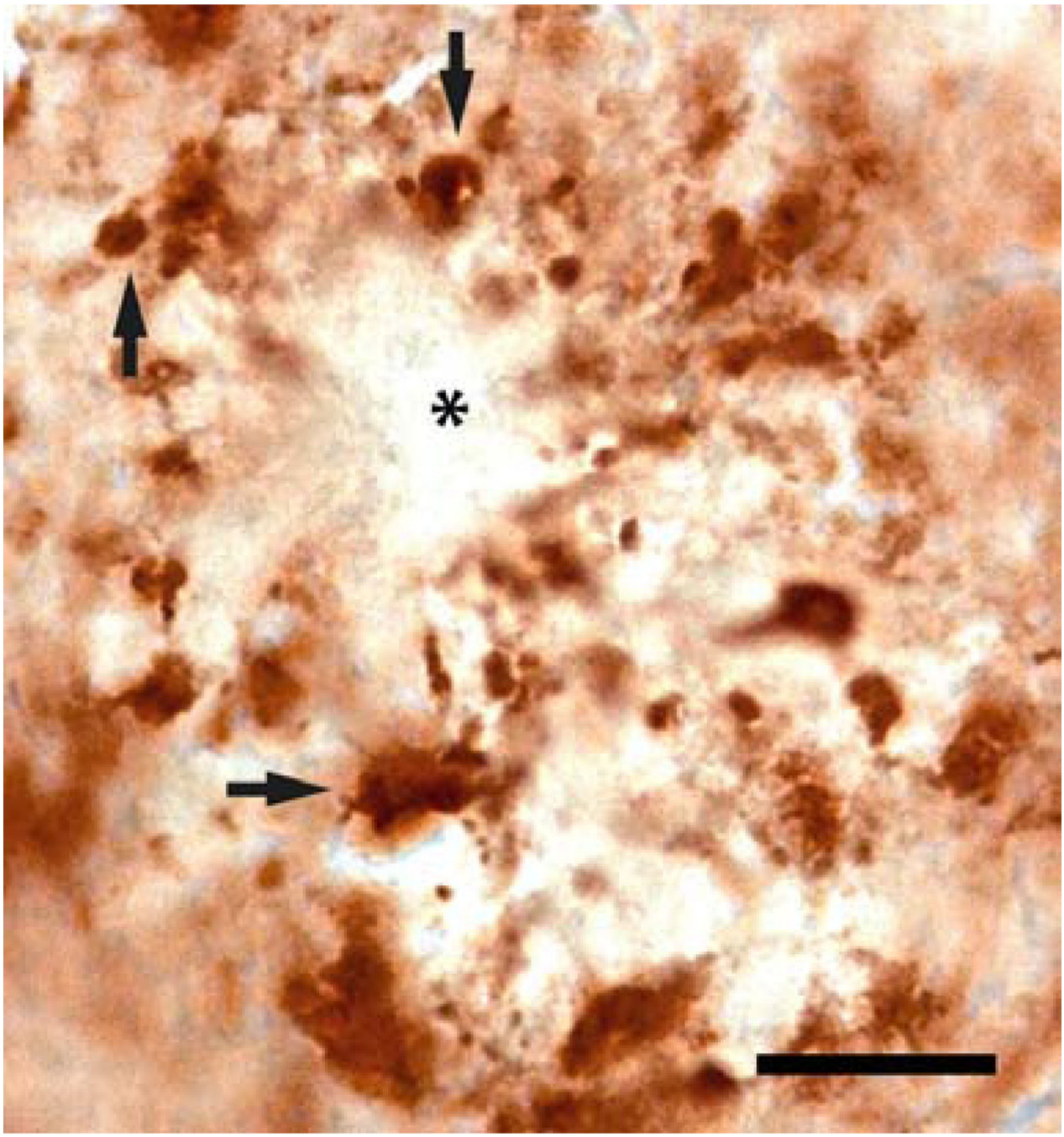

Figure 8.

High magnification of synaptophysin immunoreactivity in the hippocampus of a 10-month-old APP^{SL}/PS1ho KI mouse, showing the diminished synaptophysin signal from the core of an amyloid deposit (asterisk). Note the enlarged SIPBs (synaptophysin-immunoreactive presynaptic boutons) surrounding the plaque (black arrows). The scale bar represents 300 μm.

Table 1

Details of the stereologic counting procedure used to evaluate total neuron numbers in the hippocampus. Obj., objective used; B and H, base and height of the unbiased virtual counting frames; Dx and Dy, distance between the unbiased virtual counting frames in orthogonal directions x and y; t, measured actual average section thickness after histologic processing; Σ CS, average sum of unbiased virtual counting frames used; Σ Q^-, average number of counted neurons; CE, average predicted coefficient of error of the estimated total neuron numbers (according to [26]). DG, granule cells in the dentate gyrus; CA3, pyramidal cells in the CA3; CA1–2, pyramidal cells in the CA1–2.

	Obj.	B [µm^2]	H [µm]	Dx [µm]	Dy [µm]	t [µm]	Σ CS	Σ Q^-	CE
DG	100×	400	4	120	120	8.2	147	843	0.034
CA3	100×	400	4	60	60	8	360	748	0.036
CA1–2	100×	400	4	75	75	7.9	319	937	0.033

Table 2

Results (p values) of general linear model univariate analysis of variance. V, volume; NN, total neuron number; SIPB, number of SIPB; DG, dentate gyrus (*stratum granulare* and *stratum moleculare*); CA1–2, area CA1–2 (*stratum pyramidale* and *stratum radiatum*); CA3, area CA3 (*stratum pyramidale* and *stratum lucidum*). P values smaller than 0.05 are shown in boldface.

Variable	P value	DG / SM	CA3 / SL	CA1–2 / SR
	Age	0.128	0.321	**0.011**
V	Genotype	0.223	0.330	0.449
	Age*Genotype	0,063	0.245	0.116
	Age	0.149	0.695	**0.008**
NN	Genotype	**0.020**	0.149	**<0.001**
	Age*Genotype	0.129	0.373	**0.004**
	Age	0.889	0.819	0.105
SIPB	Genotype	**0.038**	0.536	**0.046**
	Age*Genotype	**0.027**	0.140	0.386